npj | Quantum Materials

www.nature.com/npjquantmats

REVIEW ARTICLE OPEN

Size effect in thermoelectric materials

Jun Mao[1,2,4], Zihang Liu[1,3,4] and Zhifeng Ren[1]

Thermoelectric applications have attracted increasing interest recently due to its capability of converting waste heat into electricity without hazardous emissions. Materials with enhanced thermoelectric performance have been reported in recent two decades. The revival of research for thermoelectric materials began in early 1990s when the size effect is considered. Low-dimensional materials with exceptionally high thermoelectric figure of merit (*ZT*) have been presented, which broke the limit of *ZT* around unity. The idea of size effect in thermoelectric materials even inspired the later nanostructuring and band engineering strategies, which effectively enhanced the thermoelectric performance of bulk materials. In this overview, the size effect in low-dimensional thermoelectric materials is reviewed. We first discuss the quantum confinement effect on carriers, including the enhancement of electronic density of states, semimetal to semiconductor transition and carrier pocket engineering. Then, the effect of assumptions on theoretical calculations is presented. Finally, the effect of phonon confinement and interface scattering on lattice thermal conductivity is discussed.

npj Quantum Materials (2016) **1,** 16028; doi:10.1038/npjquantmats.2016.28; published online 9 December 2016

INTRODUCTION

Thermoelectric materials are capable of converting heat into electricity and vice versa by utilising the Seebeck effect and Peltier effect, respectively.[1–3] Thermoelectric energy conversion efficiency is determined by Carnot efficiency and the dimensionless figure of merit (*ZT*), which is defined as $ZT = (S^2\sigma/\kappa)T$, where S is the Seebeck coefficient, σ the electrical conductivity, κ the thermal conductivity and T the absolute temperature. To achieve a higher *ZT* has always been the motivation for the research of thermoelectrics, however, due to strong coupling of thermoelectric parameters S, σ and κ, improving one normally leads to the deterioration of other two and finally yields negligible enhancement of *ZT*.[4]

Research of thermoelectrics advanced rapidly in 1950s, when the basic science of thermoelectrics became well established. During this period, Bi_2Te_3 compounds and its alloys had been discovered and reported to have the highest *ZT* around unity. Over the following four decades or so, there was no big development in the thermoelectric field, therefore $ZT \approx 1$ had been regarded as the benchmark for advanced thermoelectrics.[5] The turning point happened in early 1990s, when Hicks and Dresselhaus[6,7] pointed out that quantum mechanics could provide a new route of designing thermoelectric materials by reducing the dimensionality. Low-dimensional materials with exceptionally high *ZT* have been presented by different groups later, which broke the limit of unity.[8–10] More importantly, the idea of quantum effect subsequently led to the significant progress of bulk thermoelectric materials via the motivated strategies of nanostructuring[11] and band engineering.[12–15] Hence, there is the new revival of research of thermoelectrics that is still going strong.

In this overview, thermoelectric materials with size effect, specifically low-dimensional materials such as nanowires, nanotubes and superlattice thin films, are reviewed from the view point of quantum confinement effect on carriers and phonons. The enhancement of density of states, semimetal to semiconductor transition and carrier pocket engineering are discussed in regards of quantum confinement on carriers. Besides, the effect of assumptions on theoretical calculations is presented. Finally, the effect of phonon confinement and interface scattering on thermal conductivity of low-dimensional materials is discussed. Interested readers are also referred to other excellent reviews on the low-dimensional thermoelectric materials.[16–20]

QUANTUM CONFINEMENT EFFECT ON CARRIERS

In low-dimensional materials, the characteristic length of materials in certain direction is comparable to the effective de Broglie wavelength of carriers. Therefore, the motion of carriers is restricted in certain directions, which means that carriers are placed in the potential wells with infinitely high walls. In this case, the electronic spectrum will be drastically changed and this is the so-called quantum size effect.

Theoretical modelling

In early models for the calculation of thermoelectric properties of 2D quantum well structures, it was assumed that electrons were in simple parabolic bands and occupied the lowest subband of quantum well. The electronic dispersion relations for a 2D system were given by

$$\varepsilon_{2D}(k_x, k_y) = \frac{\hbar^2 k_x^2}{2m_x} + \frac{\hbar^2 k_y^2}{2m_y} + \frac{\hbar^2 \pi^2}{2m_z d_W^2} \quad (1)$$

where d_W was the width of quantum well, and m_x, m_y and m_z were the effective mass tensor components of the constant energy surfaces. It was further assumed that the current flow was in x direction and that quantum confinement was in z direction. The

[1]Department of Physics and Texas Center for Superconductivity, University of Houston, Houston, TX, USA; [2]Department of Mechanical Engineering, University of Houston, Houston, TX, USA and [3]National Key Laboratory for Precision Hot Processing of Metals and School of Materials Science and Engineering, Harbin Institute of Technology, Harbin, China.
Correspondence: Z Ren (zren@uh.edu)
[4]These authors contributed equally to this work.
Received 19 August 2016; revised 24 October 2016; accepted 3 November 2016

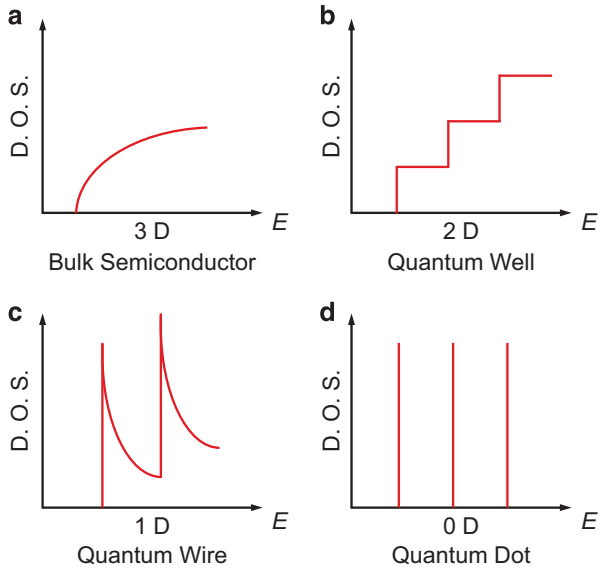

Figure 1. Electronic density of states for (**a**) a bulk semiconductor, (**b**) a 2D quantum well, (**c**) a 1D nanowire or nanotube and (**d**) a 0D quantum dot. (Adapted with permission from ref. 20).

corresponding relation used for a square 1D quantum wire was

$$\varepsilon_{1D}(k_x) = \frac{\hbar^2 k_x^2}{2m_x} + \frac{\hbar^2 \pi^2}{2m_y d_W^2} + \frac{\hbar^2 \pi^2}{2m_z d_W^2} \quad (2)$$

where the current flow was along the x direction, and quantum confinement occurred in y and z directions. Solutions of Boltzmann's equation were obtained for the thermoelectric parameters of both 2D and 1D systems.[16]

Quantum confinement effect on electronic density of states

Dimensionality plays a fundamental role in controlling the properties of materials. When the dimension of materials decreases and approaches nanometre length scales, it is possible to cause marked change in electronic density of states as shown in Figure 1.[20]

New strategy of designing thermoelectric materials by controlling the dimensionality was first discussed by Hicks and Dresselhaus.[6,7] The calculation showed that Bi_2Te_3 with quantum well (two-dimension) or quantum wire (one-dimension) structure can have the potential to reach a significantly high ZT (Figure 2). The maximum ZT increased monotonically with the decrease of characteristic length (thickness for quantum well or diameter for quantum wire).

The origin for the enhancement of thermoelectric performance mainly comes from the improved Seebeck coefficient due to the enhanced electronic density of states. According to the Mott expression (Equation (3)), S depends on the energy derivative of energy-dependent electrical conductivity $\sigma = n(E)q\mu(E)$ taken at Fermi energy E_F,[12] with $n(E) = g(E)f(E)$, the carrier density at the energy level E considered, where $g(E)$ is the density of states per unit volume and per unit energy, $f(E)$ is the Fermi function, q the carrier charge and $\mu(E)$ the mobility:

$$S = \frac{\pi^2 k_B}{3\ q} k_B T \left\{ \frac{\mathrm{d}[\ln(\sigma(E))]}{\mathrm{d}E} \right\}_{E=E_F} = \frac{\pi^2 k_B}{3\ q} k_B T \left\{ \frac{1}{n}\frac{\mathrm{d}n(E)}{\mathrm{d}E} + \frac{1}{\mu}\frac{\mathrm{d}\mu(E)}{\mathrm{d}E} \right\}_{E=E_F} \quad (3)$$

Equation (3) shows there are two mechanisms that can increase S: (i) an increased energy-dependence of $\mu(E)$, for instance by a scattering mechanism that strongly depends on the energy of charge carriers, or (ii) an increased energy-dependence of $n(E)$, for instance by a local increase in $g(E)$. For low-dimensional materials, enhancement in Seebeck coefficient mainly comes from the second mechanism. This concept can also be expressed in terms of density of state effective mass m_d^*, as shown for degenerate semiconductors:[12]

$$S = \frac{8\pi^2 k_B^2 T}{3qh^2} m_d^* \left(\frac{\pi}{3n}\right)^{2/3} \quad (4)$$

with

$$m_d^* = \left(\frac{g(E)\hbar^3\pi^2}{\sqrt{2E}}\right)^{3/2} \quad (5)$$

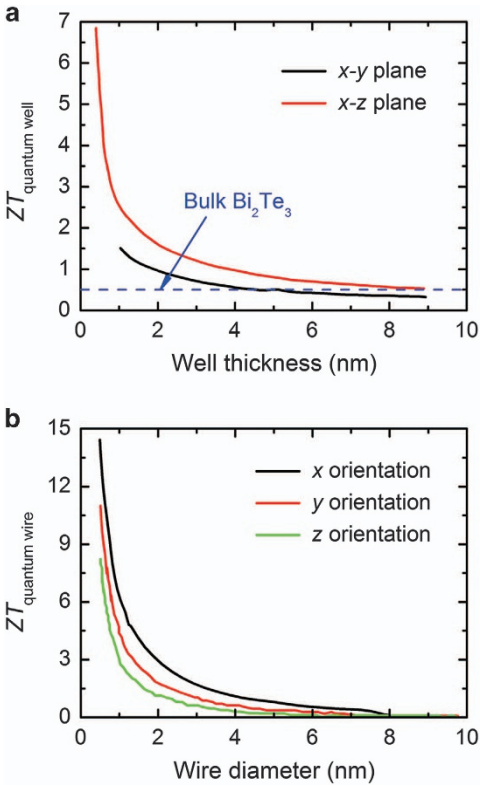

Figure 2. (**a**) ZT of quantum well as a function of the layer thickness, (**b**) ZT of quantum wire as a function of the diameter. (Adapted with permission from refs 6 and 7).

Theoretical predictions about the enhancement in Seebeck coefficient have been extensively reported in low-dimensional materials, e.g., 2D quantum well superlattice[9,21–33] and 1D quantum wire.[34–38] Here, some representative examples are presented. Harman *et al.*[21] prepared the $Pb_{1-x}Eu_xTe/PbTe$ multiple quantum wells (MQWs) with well width of ~20 Å. The measured Seebeck coefficient of MQWs was higher than that of bulk material, hence resulting in improved power factor. Hicks *et al.*[22] reported that with the decrease of well thickness from 55 to 17 Å for $Pb_{1-x}Eu_xTe/PbTe$ MQWs, the material parameter 'S^2n' (n is carrier concentration) increased by a factor of ~3 compared with that of bulk PbTe (Figure 3a and b). Harman *et al.*[25] measured the thermoelectric properties of $PbTe_{1-x}Se_x/PbTe$ quantum dot superlattice (QDS). The Seebeck coefficient of QDS was also much higher than the value calculated from the S versus n relationship of the bulk counterpart (Figure 3c and d). Ohta *et al.*[31] reported that when decreasing the thickness of quantum well to only one

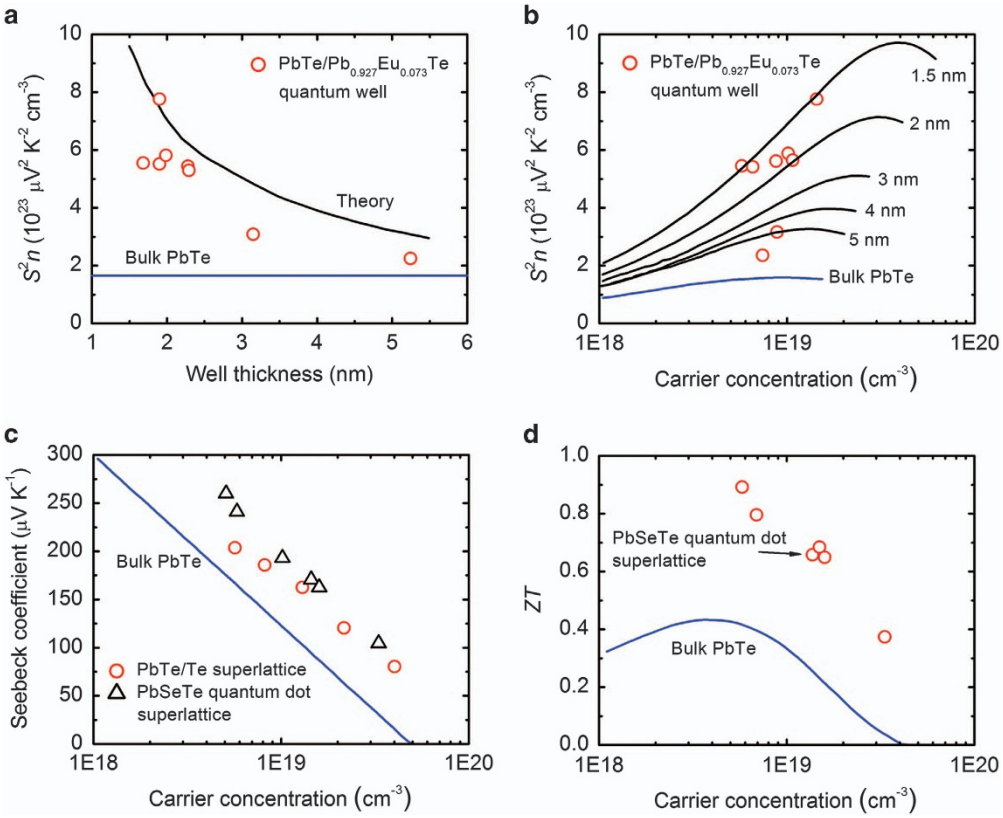

Figure 3. (**a**) S^2n of PbTe/$Pb_{0.927}Eu_{0.073}$Te quantum wells as a function of well thickness at 300 K, (**b**) S^2n of PbTe/$Pb_{0.927}Eu_{0.073}$Te quantum wells as a function of carrier concentration at 300 K, (**c**) Seebeck coefficient as a function of carrier concentration for n-type PbTe-based quantum wells and (**d**) *ZT* as a function of carrier concentration of n-type PbTe-based quantum wells. (Adapted with permission from refs 22 and 23).

unit cell layer, the Seebeck coefficients of $SrTiO_3$ superlattice was approximately five times larger than that of bulk specimen. Boukai *et al.*[34] fabricated single-crystalline Si nanowires with different diameter sizes and boron doping concentrations. The Seebeck coefficient of 10-nm-wide Si nanowires with proper carrier concentration was much higher than that of bulk Si. Wang *et al.*[32] reported that PbSe nanocrystal superlattice with varying nanocrystal sizes exhibited a significant enhancement in Seebeck coefficient compared with the bulk material. Zuev *et al.*[36] reported that when decreasing the diameter of Sb_2Te_3 nanowire from 95 to 22 nm, the Seebeck coefficient of nanowire showed an enhancement of more than 30% from 81 to 111 $\mu V\,K^{-1}$. Ohta *et al.*[39] fabricated the field effect transistor structure on a $SrTiO_3$ crystal. By applying the electric field, a 2D electron gas was formed at the gate insulator/thermoelectric materials interface, hence the Seebeck coefficient was enormously enhanced compared with the bulk one. Shimizu *et al.*[40] prepared the electric double-layer transistors based on single-wall carbon nanotube films. Their results showed that by tuning the gate bias voltage, Seebeck coefficient can be effectively enhanced. Similar results were also reported by Saito *et al.*[41] in black phosphorus. Shimizu *et al.*[42] measured the thermoelectric properties of ZnO-based ion-gated transistor. Their results showed that the thermoelectric performance of gate-tuned 2D electron gas system formed at the surface of ZnO was significantly higher than that of the bulk specimen.

Actually, similar idea of enhancing the electronic density-of-states has also been achieved later in bulk materials by introducing the resonant level from dopants.[12,15] Noticeable enhancements in Seebeck coefficient have been observed, which has effectively boosted the thermoelectric performance.[12,43–45]

Quantum confinement effect on electronic bands

Semimetal to semiconductor transition. Semimetals have the overlapped valence and conduction bands, thus electrons and holes can both participate in transport process. Due to the different signs of Seebeck coefficient for electrons and holes, semimetals always have a much lower Seebeck coefficient comparing with that of semiconductors.

However, spatial confinement of carriers by reducing the dimensionality could shift the band-edge energies, which offers the possibility of tuning band structure and enables the transition from semimetals to semiconductors. For example, when the quasi-1D electron gas for the Bi nanowires is confined inside a cylindrical potential well, the energy levels E_{ij} that electrons (and also holes) can occupy are quantised due to the quantisation of transverse momentum, so that E_{ij} can be determined by

$$E_{ij} = \frac{\hbar^2 k_x^2}{2m_x^*} + \frac{\hbar^2 \chi_{ij}^2}{2m_d^* r_0^2} \qquad (6)$$

where $2\pi\hbar = h$ is Planck's constant, k_x and m_x^* are the momentum and effective mass components of electron (or hole) along the wire axis, m_d^* is the effective mass in the plane perpendicular to wire, r_0 is the radius of wire and χ_{ij} are roots of the Bessel function $J_i(\chi_{ij}) = 0$. The quantisation of electron and hole energy levels in *y* and *z* directions makes the energy positions of the electron and hole subbands dependent on both the diameter and crystal orientation of the wire.[46]

Theoretical calculation on the semimetal to semiconductor transition of Bi was first reported by Hicks *et al.*,[7] their results showed that by reducing the diameter of quantum wire, the semimetallic Bi could be converted into a semiconductor. Later,

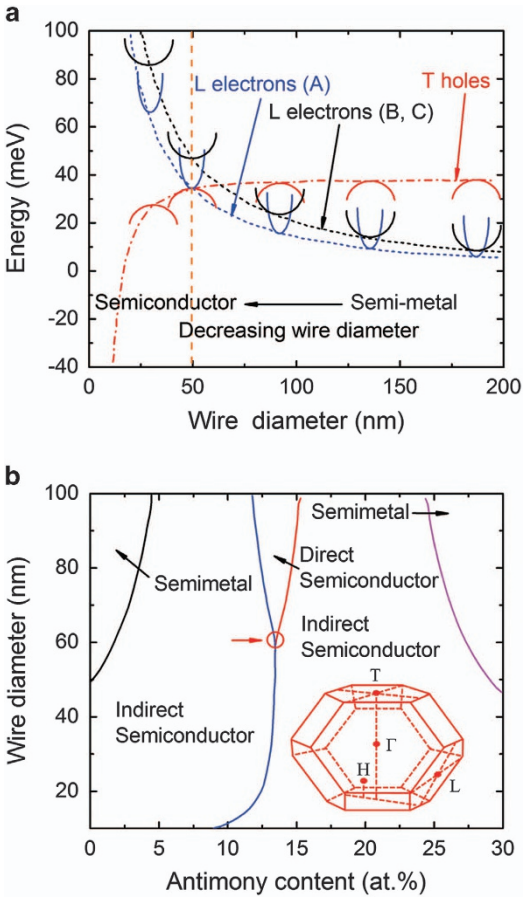

Figure 4. (**a**) The electronic band structure of Bi quantum wires showed the energy versus wire diameter of the highest subbands for the *T*-point hole carrier pocket as well as for the *L*-point electron carrier pockets, (**b**) phase horizontal diagram of the electronic band structure of $Bi_{1-x}Sb_x$ nanowires. The centre point at the condition where the 10 hole pockets coalesce in energy. (Adapted with permission from refs 47 and 54).

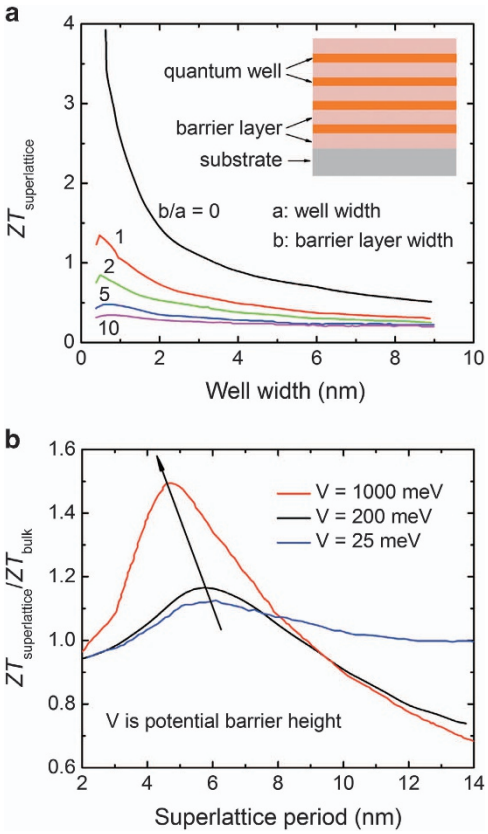

Figure 5. (**a**) *ZT* of superlattice composed of quantum wells of Bi_2Te_3 and barrier layers of $Pb_{0.75}Sn_{0.25}Te$ as a function of ratio *b*/*a*, where *a* is the thickness of quantum well and *b* is the thickness of barrier layer, (**b**) figure of merit *ZT* of Bi_2Te_3 superlattice (scaled by ZT_{bulk}) as a function of the superlattice period for several potential barrier heights. (Adapted with permission from refs 56 and 58).

Lin *et al.*[47] recalculated the thermoelectric properties of cylindrical Bi nanowire. The band edge of *L*-point electrons increased with the decreasing of wire diameter, while the highest subband edges of *T*-point holes moved downward in energy as shown in Figure 4a. At certain wire diameter (~49 nm), the energy of the lowest *L*-point conduction subband edge exceeded that of the highest *T*-point valence subband edge, indicating that these nanowires have become semiconducting. Following experimental work reported the measured electrical properties of $Bi_{1-x}Sb_x$ nanowires and observed the semimetal to semiconductor transition that showed a good agreement with previous theoretical predictions.[48–50]

Carrier pocket engineering. The process by which low-dimensional superlattices of given constituents are designed to optimise their thermoelectric properties has been called carrier pocket engineering.[51,52] In this approach, the width of barrier layers is greatly reduced and become comparable to that of quantum well, so that the wave functions of electrons are no longer confined to the quantum wells, and the carrier confinement conditions are relaxed.[53]

Due to the anisotropy of band structure, the best thermoelectric performance will only occur at certain direction. Therefore, for low-dimensional materials, better thermoelectric properties can be obtained by controlling the growth direction. Further tuning the lattice period and layer thickness, the relative contribution of different bands to the total thermoelectric performance can be controlled. Koga *et al.*[51] calculated the thermoelectric properties of GaAs/AlAs superlattice. The calculated *ZT* for Γ-point superlattice can be 10 times higher than that of bulk GaAs. Contributions from the quantum well at *X* and *L*-points in Brillouin zone can further enhance the *ZT*. Similarly, the calculated thermoelectric properties of Si/Ge superlattice showed that due to the lattice mismatch between Si and Ge, the lattice strain can offer another freedom of controlling the band structure of Si/Ge superlattice[52]

Apart from the carrier pocket engineering that can control the relative contribution of different subbands, it is also possible to align multiple carrier pockets in low-dimensional materials. This idea is quite similar to the band convergence that demonstrated in bulk materials recently.[13,14] Rabina *et al.*[54] calculated the thermoelectric properties of $Bi_{1-x}Sb_x$ nanowire. The results showed that for the p-type $Bi_{1-x}Sb_x$, the valence subband extrema occurred at three *L*-points, one *T*-point and six *H*-points of the Brillouin zone. The enhancement of *ZT* was observed near the merging of edges of ten hole pockets (the centre point as indicated by the red horizontal arrow), and along the boundary between the two indirect gap semiconductor phases as shown in Figure 4b. These degeneracies led to an increased density of states near the Fermi energy for valence band carriers in p-type $Bi_{1-x}Sb_x$, which in turn was manifested by exceptionally high *ZT*.

Effect of assumptions on theoretical calculations

In the early calculations reported by Hicks *et al.*,[6,7] simplified assumptions have been made and huge enhancements in *ZT* on the order of ~10 were predicted. Although, the following experimental work has shown some improvements in *ZT*, such a huge enhancement has never been experimentally achieved. Actually, theoretical work reported by other researchers showed that the increase in *ZT* would be significantly lower when considering more realistic assumptions. In the following part, the effect of assumptions, including the barrier layer width, potential barrier heights and the constant relaxation time approximation, on the calculated *ZT* are discussed.

Finite barrier width versus zero barrier width. The parasitic effect of barrier layer (the structure of superlattice is shown in the inset of Figure 5a, the orange layer is the quantum well and the pink layer is the barrier layer) on the thermoelectric properties was ignored in early calculations,[6,7] which was equivalent to assume the barrier layer has zero width. However, although the barrier layers do not contribute to electronic transport, they inevitably conduct heat. In order to be more realistic, Mahan and Lyon[55] calculated the thermoelectric performance of superlattice by considering the effect of barrier layer. The results showed that since barrier layer could conduct heat from the hot end to cold end, it was detrimental to the efficiency of thermoelectric devices. Similar results were also obtained by Lin-Chung and Reinecke[56] that *ZT* decreased substantially when considering the finite barrier thickness as shown in Figure 5a.

Infinite potential offset versus finite potential offset. Tunnelling of carriers through the barrier layer becomes possible when the potential offset is finite, therefore it is necessary to take the tunnelling effect into consideration for a more realistic theoretical calculation. Sofo and Mahan[57] calculated the thermoelectric properties of the superlattice with the electric field and thermal gradient applied parallel to the interfaces. Tunnelling of electrons led to the quantum mixing between quantum wells and produced a broadening of the lowest subband. It changed the density of states from a two-dimensional shape to a three-dimensional one. As a result, they found that there was a moderate increase in *ZT* with the decrease of the period of superlattice, however further reduction of the period reduced the figure of merit. Broido and Reinecke[58,59] calculated the thermoelectric properties of superlattice within the envelope-function approach. The results showed that power factor (*PF*) and *ZT* have maxima as a function of superlattice period and they can be larger than that of bulk. For superlattice period near the maximum *PF* and *ZT*, its enhancement over the bulk value was larger for larger barrier height as shown in Figure 5b. Broido and Reinecke[60] also calculated the thermoelectric properties of quantum wire superlattice and the electron tunnelling showed significant effect on the calculated results as well.

Constant relaxation time approximation versus fully considering of elastic and inelastic carrier scattering. The constant relaxation time approximation (CRTA) assumes that the carrier scattering time is independent of carrier energy and well thickness or wire diameter. However, the electron scattering rates in superlattice differ qualitatively from those in bulk materials. This gives rise to the decreased carrier mobility with decreasing well thickness.[61] Broido and Reinecke[61] developed a full theory of thermoelectric transport in superlattice, included the well width and energy dependence of the optical and acoustic phonon scattering. The results showed that with the decreasing of quantum well thickness, the increased carrier-phonon scattering rates led to more modest increase in *ZT* than predicted by constant relaxation time approximation. Later, Broido and Reinecke[62] calculated the thermoelectric power factor for quantum well and quantum wire superlattice. The dependence of *PF* on potential offset *V* was found to be qualitatively weaker than in previous work based on the constant relaxation time approximation for carrier scattering. It was evident that the relaxation time approximation gave a significantly higher *PF* than that obtained from the inelastic calculation as shown in Figure 6.

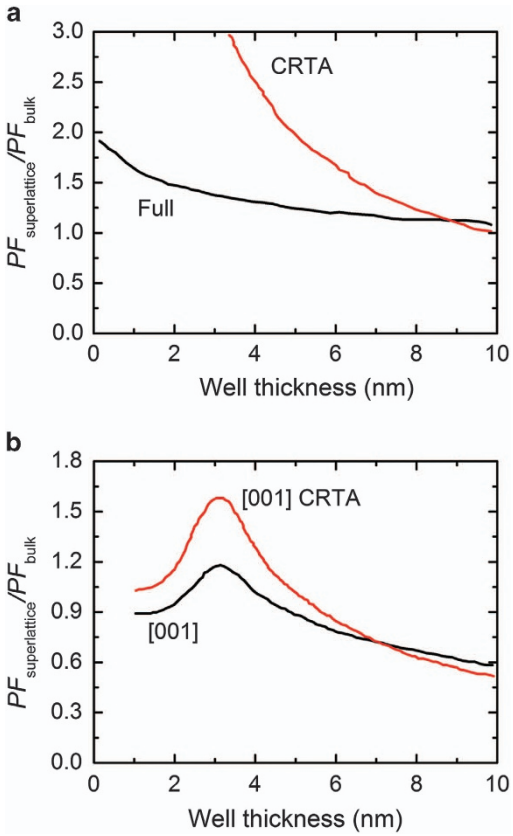

Figure 6. (**a**) Well-width dependence of *PF* for PbTe [001] quantum well superlattice with infinite barrier height scaled to corresponding bulk *PF*. Black solid line is full calculation and red solid line is from constant relaxation time approximation (CRTA), (**b**) *PF* for PbTe quantum superlattice grown in the [001] (black solid line) for potential offsets $V = 1{,}000$ meV, well width equal to barrier width. Red solid line is for PbTe [100] in the CRTA. (Adapted with permission from ref. 59).

QUANTUM CONFINEMENT EFFECT ON PHONONS AND INTERFACE SCATTERING

The quantum confinement effect on carriers led to the enhancement in *PF* as mentioned above. Similar phonon quantum confinement effect was also observed and hence strong modification of phonon group velocity occurred.[63,64] Besides, the interface scattering became significant when the dimension of materials was reduced.[65–67] Therefore, it was reported that *ZT* can be further enhanced from the reduction of lattice thermal conductivity in a wide variety of thermoelectric systems.[8,9,27,29,34,35,68–93]

Yao[68] measured the thermal conductivity of AlAs/GaAs superlattice, which showed a reduction with the decrease of layer thickness. A similar reduction of in-plane thermal conductivity was also reported in the $PbTe/PbSe_{0.2}Te_{0.8}$ superlattice compared with that of bulk materials.[74] In addition, the in-plane thermal conductivity of the 50-period Ge/Si quantum dot superlattice was measured and the room temperature value was ~30.5 $W\,m^{-1}\,K^{-1}$, much smaller than that of bulk Si.[72] Venkatasubramanian *et al.*[8]

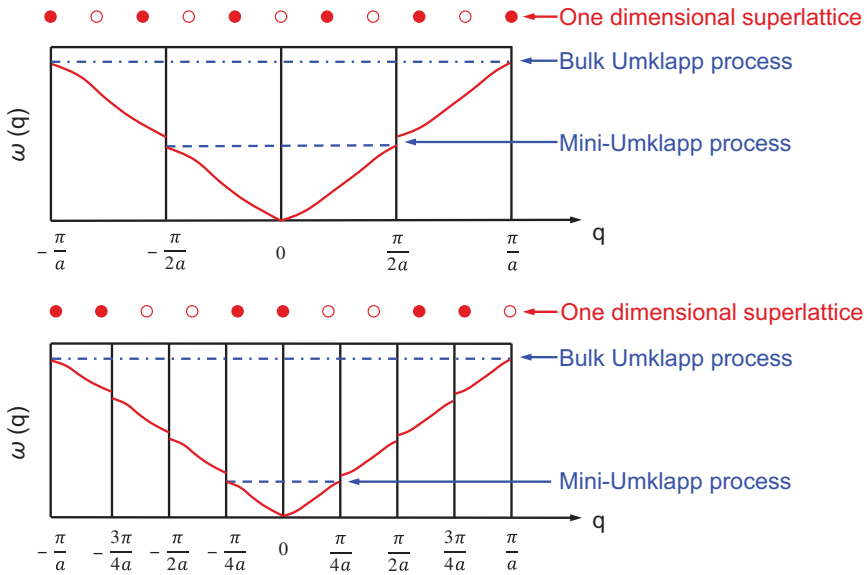

Figure 7. Brillouin zone of the superlattice, the dash-dotted lines are the bulk Umklapp process wavevectors and the dash lines are the smallest mini-Umklapp process wavevectors.

measured the thermoelectric properties of p-type Bi_2Te_3/Sb_2Te_3 superlattice which showed a *ZT* of ~2.5 at ambient temperature. The high *ZT* was ascribed to the phonon blocking/electron transmitting structure in which the lattice thermal conductivity was reduced significantly. However, it should be noted that the direction for the measured thermal conductivity is questionable. Boukai *et al.*[34] reported that thermal conductivity of single-crystalline Si nanowires decreased obviously with the decrease of nanowire diameter and the thermal conductivity of 10 nm in diameter nanowires was only $\sim 0.76 \pm 0.15$ W m^{-1} K^{-1}. It led to a large enhancement of *ZT* and the highest value was an ~100-fold that of bulk Si. Roh *et al.*[79] reported the thermal conductivities of individual single-crystalline PbTe nanowires decreased with the reduction of wire diameter. Similarly, PbSe nanowires with the diameter ranging from 50 to 100 nm exhibited a noticeable reduction in thermal conductivity.[77] Besides, the thermal conductivity of Bi single-crystalline nanowires decreased gradually with the decrease of diameter from 310 to 40 nm.[70] The thermal conductivity of thin film is measured by the 3ω technique,[94] while for one-dimensional materials (i.e., nanotubes and nanowires), thermal conductivity is measured by using micro-fabricated devices.[95,96] Due to the small contact area between the low-dimensional materials and measurement device, the contact thermal resistance could lead to a large measurement uncertainty.

In order to further understand the reason of reduction in lattice thermal conductivity in low-dimensional materials, phonon confinement and interface scattering are discussed.

Quantum confinement effect on phonons

When the dimension of nanostructures reduces to a critical value, phonon confinement effects must be considered. The first theoretical calculation on thermal conductivity of superlattice was conducted by Ren and Dow.[97] Different from the bulk material, the lattice thermal conductivity of superlattice depended upon a new kind of Umklapp scattering process, called a mini-Umklapp, associated with the mini-Brillouin zone of superlattice as shown in Figure 7. The superlattice consisting of periodically alternating layers of material has a large superlattice constant and hence a small or mini-Brillouin zone in the direction of layering. The mini-reciprocal-lattice vectors associated with this mini-zone gave rise to mini-Umklapp processes which contributed to the thermal resistance.

Later, Balandin and Wang[64,98] investigated the phonon confinement in quantum wells. Strong modification of phonon group velocities due to the quantum confinement led to a significant increase in the phonon relaxation rates, thus reduced the thermal conductivity. Hyldgaard and Mahan[63] investigated the phonon supperlattice transport. Total internal reflection confined the superlattice modes and significantly reduced the average group velocity. The consequences of acoustic mismatch led to an order-of-magnitude reduction in the ratio of thermal conductivity to phonon relaxation time. Tamura and Tanaka[99] pointed out that the reduced group velocity near the folded Brillouin-zone centre and edges yields a reduction in thermal conductivity that is less than the experimentally measured values in Si/Ge and GaAs/AlAs superlattices. Therefore, phonon confinement and the associated group velocity reduction are the causes of the observed drop in the cross-plane thermal conductivity of semiconductor superlattices. Khitun *et al.*[100] calculated the thermoelectric transport properties of quantum dot superlattice. The model for calculation took into account of electron and phonon transport modifications due to the quantum confinement caused by the mismatch in electronic and thermal properties between dot and host materials. The results showed that the predicted enhancement in *ZT* was mainly due to the significant drop in lattice thermal conductivity caused by the acoustic phonon scattering by quantum dots. For quantum wire, Khitun *et al.*[101] predicted that the majority of heat in silicon nanowire is carried by acoustic phonons with wavevectors close to Brillouin zone centre. Due to phonon confinement effect, the decrease of lattice thermal conductivity in quantum wires is stronger than in quantum wells of corresponding dimensions and this does not differ significantly for free- or clamped-surface boundaries.

Interface scattering

The reduced dimensionality of materials increases the possiblity of interface scattering of phonons, which also has a significant effect on the lattice thermal conductivity. It should be pointed out that the phonon mean free path (MFP) has a critical role in the interface scattering. When the phonon MFP is comparable to the characteristic length of interfaces, significant phonon scattering by

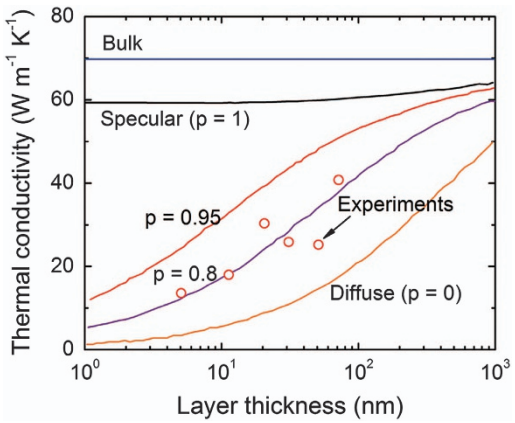

Figure 8. Thermal conductivity as a function of the layer thickness for GaAs/AlAs superlattices of equal layer thickness at room temperature.

interfaces can be expected. For some materials with intrinsically low thermal conductivity, i.e., with very short phonon MFP, the interface scattering will not be very effective.

Chen[65] investigated the interface effects on thermal conductivity of superlattice and periodic thin-film structure. Different interface conditions including specular, diffuse, and partially specular and partially diffuse interfaces were considered. Results obatined from the partially specular and partially diffuse interface scattering model showed a good agreement with experimental data of GaAs/AlAs superlattice as shown in Figure 8. The study showed that the atomic scale interface roughness was the major cause for the measured reduction in thermal conductivity.

The interface scattering in superlattice is thickness dependent, below the critical thickness, thermal conductivity was strongly influenced by diffuse interface scattering of phonons while above the critical thickness, dislocations were the dominant scattering centres in superlattice. These experiments showed that the thermal conductivity of superlattice structures were generally lower than the values calculated from the thermal conductivity of their constituting single crystal materials according to Fourier heat conduction theory. When the layers were very thin and scattering at the interfaces was totally diffuse, the temperature drop inside each layer was small compared with the temperature drop at the interface.[66] The effective thermal conductivity of superlattice in the perpendicular direction was generally controlled by phonon transport within each layer and the thermal boundary resistance (TBR) between different layers. The TBR was no long an intrinsic property of the interface, but depends on the layer thickness as well as the phonon mean free path. In the thin layer limit, phonon transport within each layer was ballistic, and the TBR dominated the effective thermal conductivity of superlattice. It was concluded that the cross-plane thermal conductivity of these superlattice was controlled by diffuse and inelastic scattering processes at interfaces.[67] Zou and Balandin[102] first developed a model for heat conduction in a semiconductor nanowire with dimensions comparable to the phonon mean free path. The result showed that by modifying the surface of nanowire, a significant decrease in lattice thermal conductivity can be obtained. Donadio and Galli[103] reported that wires with amorphous surfaces have the smallest value, about 100 times lower than that of the bulk. This is because of a reduction of propagating mode lifetimes at the crystalline–amorphous interface, in combination with the presence of non-propagating, diffusive modes similar to those found in α-Si. Later, Liu and Chen[104] demonstrated that incorporating roughness by patterning (or etching) may further reduce the thermal conductivity to a significant extent for silicon nanowires using molecular dynamics simulations. The roughness effect is more prominent when the nanowire is longer and thicker. Hopkins *et al.*[81] demonstrated that the obvious reduction of cross-plane thermal conductivity in SiGe quantum dot superlattices is primarily due to the increased physical roughness at the superlattice interfaces.

Even though quantum size effect is significant, how to realise its full potential in bulk materials is a daunting challenge. In order to realise quantum size effect in bulk materials, it is necessary to reduce the grain size to a critical value. However, current nanostructuring technique is unable to synthesise bulk materials with average grain sizes of ~10 nm or smaller (slightly larger than the electron mean free path). If such a small grain size could be achieved, significant phonon scattering by grain boundary could be expected and a much higher thermoelectric performance is possible. Introducing grain growth inhibitors could be one of the possible approaches, these inhibitors themselves should not interfere the electron transport and should also have very low thermal conductivity. Low-temperature consolidation of nanopowders could be another possibility of obtaining bulk materials with extremely small grain sizes. However, the prepared specimens will be limited to low-temperature thermoelectric application in order to prevent grain growth. Besides, it is noted that the nanostructures of low-dimensional materials, e.g., superlattice and nanowire superlattice, are highly desirable. Although bulk materials with random nanostructures demonstrate good thermoelectric materials, it is reasonable to believe that bulk materials with highly ordered nanostructures could have much higher carrier mobility, therefore they have the potential to achieve a very high thermoelectric performance. To synthesise the bulk materials with highly ordered nanostructures, preferred orientation of nanopowders by external fields (e.g., magnetic field, electrical field) could be one of the possible methods. Modulation doping could be another promising method if the particles can be truly isolated without reacting with the matrix during the sample preparation but only provide the needed electrons or holes.[105,106]

Conclusion

In this review, the quantum thermoelectric materials were discussed. The radical change of the electronic density of state by reducing the dimensionality of materials was presented. It led to the enhancement of Seebeck coefficient, and enabled the semimetal to semiconductor transition and carrier pocket engineering. Moreover, the effect of assumptions on the calculated thermoelectric properties was presented. Finally, the effect of phonon confinement and the interface scattering on the reduction of lattice thermal conductivity was also discussed.

ACKNOWLEDGEMENTS

This work was funded by the US Department of Energy under Contract No. DE-SC0010831 and also partially by 'Solid State Solar Thermal Energy Conversion Center (S^3TEC)', an Energy Frontier Research Center funded by the US Department of Energy, Office of Science, Office of Basic Energy Science under award number DE-SC0001299.

COMPETING INTERESTS

The authors declare no conflict of interest.

REFERENCES

1. DiSalvo, F. J. Thermoelectric cooling and power generation. *Science* **285**, 703–706 (1999).
2. Bell, L. E. Cooling heating, generating power, and recovering waste heat with thermoelectric systems. *Science* **321**, 1457–1461 (2008).
3. Snyder, G. J. & Toberer, E. S. Complex thermoelectric materials. *Nat. Mater.* **7**, 105–114 (2008).
4. Ioffe A. F. (eds) *Semiconductor Thermoelements and Thermoelectric Cooling*. Infosearch, (1957).

5. Rowe D. M. (eds) *CRC Handbook of Thermoelectrics*. CRC press, (1995).
6. Hicks, L. & Dresselhaus, M. Thermoelectric figure of merit of a one-dimensional conductor. *Phys. Rev. B* **47**, 16631–16634 (1993).
7. Hicks, L. D. & Dresselhaus, M. S. Effect of quantum-well structures on the thermoelectric figure of merit. *Phys. Rev. B* **47**, 12727–12731 (1993).
8. Venkatasubramanian, R., Siivola, E., Colpitts, T. & O'Quinn, B. Thin-film thermoelectric devices with high room-temperature figures of merit. *Nature* **413**, 597–602 (2001).
9. Harman, T. C., Taylor, P. J., Walsh, M. P. & LaForge, B. E. Quantum dot superlattice thermoelectric materials and devices. *Science* **297**, 2229–2232 (2002).
10. Harman, T., Walsh, M. & Turner, G. Nanostructured thermoelectric materials. *J. Electron. Mater.* **34**, L19–L22 (2005).
11. Poudel, B. *et al.* High-thermoelectric performance of nanostructured bismuth antimony telluride bulk alloys. *Science* **320**, 634–638 (2008).
12. Heremans, J. P. *et al.* Enhancement of thermoelectric efficiency in PbTe by distortion of the electronic density of states. *Science* **321**, 554–557 (2008).
13. Pei, Y. *et al.* Convergence of electronic bands for high performance bulk thermoelectrics. *Nature* **473**, 66–69 (2011).
14. Liu, W. *et al.* Convergence of conduction bands as a means of enhancing thermoelectric performance of n-Type $Mg_2Si_{1-x}Sn_x$ solid solutions. *Phys. Rev. Lett.* **108**, 166601 (2012).
15. Heremans, J. P., Wiendlocha, B. & Chamoire, A. M. Resonant levels in bulk thermoelectric semiconductors. *Energy Environ. Sci.* **5**, 5510–5530 (2012).
16. Dresselhaus, M. *et al.* Low-dimensional thermoelectric materials. *Phys. Solid State* **41**, 679–682 (1999).
17. Dresselhaus, M. *et al.* The promise of low-dimensional thermoelectric materials. *Microscale Therm. Eng.* **3**, 89–100 (1999).
18. Dresselhaus, M. *et al.* Quantum wells and quantum wires for potential thermoelectric applications. *Semicond. Semimet.* **71**, 1–121 (2001).
19. Böttner, H., Chen, G. & Venkatasubramanian, R. Aspects of thin-film superlattice thermoelectric materials, devices, and applications. *MRS Bull.* **31**, 211–217 (2006).
20. Dresselhaus, M. S. *et al.* New directions for low-dimensional thermoelectric materials. *Adv. Mater.* **19**, 1043–1053 (2007).
21. Harman, T. C., Spears, D. L. & Manfra, M. J. High thermoelectric figures of merit in PbTe quantum wells. *J. Electron. Mater.* **25**, 1121–1127 (1996).
22. Hicks, L. D., Harman, T. C., Sun, X. & Dresselhaus, M. S. Experimental study of the effect of quantum-well structures on the thermoelectric figure of merit. *Phys. Rev. B* **53**, 10493–10496 (1996).
23. Harman, T., Taylor, P., Spears, D. & Walsh, M. in *Proceedings of International Conference on Thermoelectrics.* 280–284 (1999).
24. Harman, T., Spears, D. & Walsh, M. PbTe/Te superlattice structures with enhanced thermoelectric figures of merit. *J. Electron. Mater.* **28**, L1–L5 (1999).
25. Harman, T. C., Taylor, P. J., Spears, D. L. & Walsh, M. P. Thermoelectric quantum-dot superlattices with high ZT. *J. Electron. Mater.* **29**, L1–L4 (2000).
26. Rogacheva, E. *et al.* Quantum size effects in PbSe quantum wells. *Appl. Phys. Lett.* **80**, 2690–2692 (2002).
27. Yang, B., Liu, J., Wang, K. & Chen, G. Simultaneous measurements of Seebeck coefficient and thermal conductivity across superlattice. *Appl. Phys. Lett.* **80**, 1758–1760 (2002).
28. Rogacheva, E. *et al.* Quantum size effects in n-PbTe/p-SnTe/n-PbTe heterostructures. *Appl. Phys. Lett.* **86**, 063103 (2005).
29. Bao, Y. *et al.* Electrical and thermal conductivity of Ge/Si quantum dot superlattices. *J. Electrochem. Soc.* **152**, G432–G435 (2005).
30. Zide, J. *et al.* Demonstration of electron filtering to increase the Seebeck coefficient in $In_{0.53}Ga_{0.47}As/In_{0.53}Ga_{0.28}Al_{0.19}As$ superlattices. *Phys. Rev. B* **74**, 205335 (2006).
31. Ohta, H. *et al.* Giant thermoelectric Seebeck coefficient of two-dimensional electron gas in $SrTiO_3$. *Nature Mater.* **6**, 129–134 (2007).
32. Wang, R. Y. *et al.* Enhanced thermopower in PbSe nanocrystal quantum dot superlattices. *Nano Lett.* **8**, 2283–2288 (2008).
33. Cecchi, S. *et al.* Ge/SiGe superlattices for thermoelectric energy conversion devices. *J. Mater. Sci.* **48**, 2829–2835 (2013).
34. Boukai, A. I. *et al.* Silicon nanowires as efficient thermoelectric materials. *Nature* **451**, 168–171 (2008).
35. Tang, J. *et al.* Holey silicon as an efficient thermoelectric material. *Nano Lett.* **10**, 4279–4283 (2010).
36. Zuev, Y. M., Lee, J. S., Galloy, C., Park, H. & Kim, P. Diameter dependence of the transport properties of antimony telluride nanowires. *Nano Lett.* **10**, 3037–3040 (2010).
37. Wu, P. M. *et al.* Large thermoelectric power factor enhancement observed in InAs nanowires. *Nano Lett.* **13**, 4080–4086 (2013).
38. Kim, J., Lee, S., Brovman, Y. M., Kim, P. & Lee, W. Diameter-dependent thermoelectric figure of merit in single-crystalline Bi nanowires. *Nanoscale* **7**, 5053–5059 (2015).
39. Ohta, H. *et al.* Unusually large enhancement of thermopower in an electric field induced two-dimensional electron gas. *Adv. Mater.* **24**, 740–744 (2012).
40. Shimizu, S. *et al.* Thermoelectric detection of multi-subband density of states in semiconducting and metallic single-walled carbon nanotubes. *Small* **12**, 3388–3392 (2016).
41. Saito, Y. *et al.* Gate-tuned thermoelectric power in black phosphorus. *Nano Lett.* **16**, 4819–4824 (2016).
42. Shimizu, S. *et al.* Enhanced thermopower in ZnO two-dimensional electron gas. *Proc. Natl Acad. Sci. USA* **113**, 6438–6443 (2016).
43. Zhang, Q. *et al.* Enhancement of thermoelectric figure-of-merit by resonant states of aluminium doping in lead selenide. *Energy Environ. Sci.* **5**, 5246–5251 (2012).
44. Zhang, Q. *et al.* High thermoelectric performance by resonant dopant indium in nanostructured SnTe. *Proc. Natl Acad. Sci. USA* **110**, 13261–13266 (2013).
45. Tan, G. *et al.* High thermoelectric performance $SnTe\text{-}In_2Te_3$ solid solutions enabled by resonant levels and strong vacancy phonon scattering. *Chem. Mater.* **27**, 7801–7811 (2015).
46. Dresselhaus, M. S. *et al.* The promise of low-dimensional thermoelectric materials. *Microscale Therm. Eng.* **3**, 89–100 (1999).
47. Lin, Y. M., Sun, X. Z. & Dresselhaus, M. S. Theoretical investigation of thermoelectric transport properties of cylindrical Bi nanowires. *Phys. Rev. B* **62**, 4610–4623 (2000).
48. Heremans, J. & Thrush, C. M. Thermoelectric power of bismuth nanowires. *Phys. Rev. B* **59**, 12579–12583 (1999).
49. Lin, Y. M., Cronin, S. B., Ying, J. Y., Dresselhaus, M. & Heremans, J. P. Transport properties of Bi nanowire arrays. *Appl. Phys. Lett.* **76**, 3944–3946 (2000).
50. Lin, Y. M., Rabin, O., Cronin, S. B., Ying, J. Y. & Dresselhaus, M. S. Semimetal-semiconductor transition in $Bi_{1-x}Sb_x$ alloy nanowires and their thermoelectric properties. *Appl. Phys. Lett.* **81**, 2403–2405 (2002).
51. Koga, T., Sun, X., Cronin, S. B. & Dresselhaus, M. S. Carrier pocket engineering to design superior thermoelectric materials using GaAs/AlAs superlattices. *Appl. Phys. Lett.* **73**, 2950–2952 (1998).
52. Koga, T., Sun, X., Cronin, S. & Dresselhaus, M. Carrier pocket engineering applied to 'strained' Si/Ge superlattices to design useful thermoelectric materials. *Appl. Phys. Lett.* **75**, 2438–2440 (1999).
53. Dresselhaus, M. S. *et al. Recent Trends in Thermoelectric Materials Research*, Vol. 71 (Elsevier, pp 1–121, 2001).
54. Rabina, O., Lin, Y. M. & Dresselhaus, M. S. Anomalously high thermoelectric figure of merit in $Bi_{1-x}Sb_x$ nanowires by carrier pocket alignment. *Appl. Phys. Lett.* **79**, 81–83 (2001).
55. Mahan, G. & Lyon, H. Jr. Thermoelectric devices using semiconductor quantum wells. *J. Appl. Phys.* **76**, 1899–1901 (1994).
56. Lin-Chung, P. & Reinecke, T. Thermoelectric figure of merit of composite superlattice systems. *Phys. Rev. B Condens. Matter.* **51**, 13244–13248 (1995).
57. Sofo, J. & Mahan, G. Thermoelectric figure of merit of superlattices. *Appl. Phys. Lett.* **65**, 2690–2692 (1994).
58. Broido, D. & Reinecke, T. Effect of superlattice structure on the thermoelectric figure of merit. *Phys. Rev. B* **51**, 13797–13800 (1995).
59. Broido, D. & Reinecke, T. Thermoelectric power factor in superlattice systems. *Appl. Phys. Lett.* **77**, 705–707 (2000).
60. Broido, D. & Reinecke, T. Thermoelectric figure of merit of quantum wire superlattices. *Appl. Phys. Lett.* **67**, 100–102 (1995).
61. Broido, D. & Reinecke, T. Thermoelectric transport in quantum well superlattices. *Appl. Phys. Lett.* **70**, 2834–2836 (1997).
62. Broido, D. & Reinecke, T. Theory of thermoelectric power factor in quantum well and quantum wire superlattices. *Phys. Rev. B* **64**, 045324 (2001).
63. Hyldgaard, P. & Mahan, G. Phonon superlattice transport. *Phys. Rev. B* **56**, 10754–10757 (1997).
64. Balandin, A. & Wang, K. L. Effect of phonon confinement on the thermoelectric figure of merit of quantum wells. *J. Appl. Phys.* **84**, 6149–6153 (1998).
65. Chen, G. Size and interface effects on thermal conductivity of superlattices and periodic thin-film structures. *J. Heat Transfer* **119**, 220–229 (1997).
66. Chen, G. & Neagu, M. Thermal conductivity and heat transfer in superlattices. *Appl. Phys. Lett.* **71**, 2761–2763 (1997).
67. Chen, G. Thermal conductivity and ballistic-phonon transport in the cross-plane direction of superlattices. *Phys. Rev. B* **57**, 14958–14973 (1998).
68. Yao, T. Thermal properties of AlAs/GaAs superlattices. *Appl. Phys. Lett.* **51**, 1798–1800 (1987).
69. Lee, S., Cahill, D. G. & Venkatasubramanian, R. Thermal conductivity of Si/Ge superlattices. *Appl. Phys. Lett.* **70**, 2957–2959 (1997).
70. Venkatasubramanian, R., Siivola, E. & Colpitts, T. in *Proceedings of International Conference on Thermoelectrics*. 191–197 (1998).
71. Lambrecht, A., Beyer, H., Nurnus, J., Künzel, C. & Böttner, H. in *Proceedings of International Conference on Thermoelectrics.* 335–339 (2001).
72. Liu, J. *et al.* Growth of Ge quantum dot superlattices for thermoelectric applications. *J. Cryst. Growth* **227**, 1111–1115 (2001).
73. Borca-Tasciuc, D. A. *et al.* Thermal conductivity of InAs/AlSb superlattices. *Microscale Therm. Eng.* **5**, 225–231 (2001).

74. Beyer, H. *et al.* PbTe based superlattice structures with high thermoelectric efficiency. *Appl. Phys. Lett.* **80**, 1216–1218 (2002).
75. Zeng, G. *et al.* ErAs: InGaAs/InGaAlAs superlattice thin-film power generator array. *Appl. Phys. Lett.* **88**, 113502 (2006).
76. Hochbaum, A. I. *et al.* Enhanced thermoelectric performance of rough silicon nanowires. *Nature* **451**, 163–167 (2008).
77. Liang, W. *et al.* Thermoelectric properties of p-type PbSe nanowires. *Nano Res.* **2**, 394–399 (2009).
78. Moore, A. L., Pettes, M. T., Zhou, F. & Shi, L. Thermal conductivity suppression in bismuth nanowires. *J. Appl.Phys.* **106**, 034310 (2009).
79. Roh, J. W. *et al.* Size-dependent thermal conductivity of individual single-crystalline PbTe nanowires. *Appl. Phys. Lett.* **96**, 103101 (2010).
80. Pernot, G. *et al.* Precise control of thermal conductivity at the nanoscale through individual phonon-scattering barriers. *Nat. Mater.* **9**, 491–495 (2010).
81. Hopkins, P. E., Duda, J. C., Petz, C. W. & Floro, J. A. Controlling thermal conductance through quantum dot roughening at interfaces. *Phys. Rev. B* **84**, 035438 (2011).
82. Zhou, C., Nguyen, B.-M., Razeghi, M. & Grayson, M. Thermal conductivity of InAs/GaSb type II superlattice. *J. Electron. Mater.* **41**, 2322–2325 (2012).
83. Hu, M. & Poulikakos, D. Si/Ge superlattice nanowires with ultralow thermal conductivity. *Nano Lett.* **12**, 5487–5494 (2012).
84. Luckyanova, M. N. *et al.* Anisotropy of the thermal conductivity in GaAs/AlAs superlattices. *Nano Lett.* **13**, 3973–3977 (2013).
85. Llin, L. F. *et al.* The cross-plane thermoelectric properties of p-Ge/$Si_{0.5}Ge_{0.5}$ superlattices. *Appl. Phys. Lett.* **103**, 143507 (2013).
86. Chang, H. T. *et al.* High quality multifold Ge/Si/Ge composite quantum dots for thermoelectric materials. *Appl. Phys. Lett.* **102**, 101902 (2013).
87. Chang, H. T., Wang, S. Y. & Lee, S. W. Designer Ge/Si composite quantum dots with enhanced thermoelectric properties. *Nanoscale* **6**, 3593–3598 (2014).
88. Sood, A. *et al.* Thermal conduction in lattice-matched superlattices of InGaAs/InAlAs. *Appl. Phys. Lett.* **105**, 051909 (2014).
89. Jaeger, T. *et al.* Thermal conductivity of half-Heusler superlattices. *Semicond. Sci. Tech.* **29**, 124003 (2014).
90. Mizuno, H., Mossa, S. & Barrat, J. L. Beating the amorphous limit in thermal conductivity by superlattices design. *Sci. Rep.* **5**, 14116 (2015).
91. Abutaha, A. I. *et al.* Enhanced thermoelectric figure-of-merit in thermally robust, nanostructured superlattices based on $SrTiO_3$. *Chem. Mater.* **27**, 2165–2171 (2015).
92. Ferrando-Villalba, P. *et al.* Tailoring thermal conductivity by engineering compositional gradients in $Si_{1-x}Ge_x$ superlattices. *Nano Res.* **8**, 2833–2841 (2015).
93. Llin, L. F. *et al.* Thermoelectric cross-plane properties on p-and n-Ge/Si_xGe_{1-x} superlattices. *Thin Solid Films* **602**, 90–94 (2015).
94. Cahill, D. G., Fischer, H. E., Klitsner, T., Swartz, E. & Pohl, R. Thermal conductivity of thin films: measurements and understanding. *J. Vac. Sci. Technol. A* **7**, 1259–1266 (1989).
95. Shi, L. *et al.* Measuring thermal and thermoelectric properties of one-dimensional nanostructures using a microfabricated device. *J. Heat Transfer* **125**, 881–888 (2003).
96. Li, D. *et al.* Thermal conductivity of individual silicon nanowires. *Appl. Phys. Lett.* **83**, 2934–2936 (2003).
97. Ren, S. Y. & Dow, J. D. Thermal conductivity of superlattices. *Phys. Rev. B* **25**, 3750–3755 (1982).
98. Balandin, A. & Wang, K. L. Significant decrease of the lattice thermal conductivity due to phonon confinement in a free-standing semiconductor quantum well. *Phys. Rev. B* **58**, 1544–1549 (1998).
99. Tamura, S.-i., Tanaka, Y. & Maris, H. J. Phonon group velocity and thermal conduction in superlattices. *Phys. Rev. B* **60**, 2627–2630 (1999).
100. Khitun, A., Wang, K. & Chen, G. Thermoelectric figure of merit enhancement in a quantum dot superlattice. *Nanotechnology* **11**, 327–331 (2000).
101. Khitun, A., Balandin, A. & Wang, K. Modification of the lattice thermal conductivity in silicon quantum wires due to spatial confinement of acoustic phonons. *Superlattices Microstruct.* **26**, 181–193 (1999).
102. Zou, J. & Balandin, A. Phonon heat conduction in a semiconductor nanowire. *J. Appl. Phys.* **89**, 2932–2938 (2001).
103. Donadio, D. & Galli, G. Atomistic simulations of heat transport in silicon nanowires. *Phys. Rev. Lett.* **102**, 195901 (2009).
104. Liu, L. & Chen, X. Effect of surface roughness on thermal conductivity of silicon nanowires. *J. Appl. Phys.* **107**, 033501 (2010).
105. Zebarjadi, M. *et al.* Power factor enhancement by modulation doping in bulk nanocomposites. *Nano Lett.* **11**, 2225–2230 (2011).
106. Yu, B. *et al.* Enhancement of thermoelectric properties by modulation-doping in silicon germanium alloy nanocomposites. *Nano Lett.* **12**, 2077–2082 (2012).